Physics Letters A 379 (2015) 732–737

Contents lists available at ScienceDirect

Physics Letters A

www.elsevier.com/locate/pla

Superconducting properties of a parallelepiped mesoscopic superconductor: A comparative study between the 2D and 3D Ginzburg–Landau models

J. Barba-Ortega [a,*], Edson Sardella [b,c], J. Albino Aguiar [d]

[a] Departamento de Física, Universidad Nacional de Colombia, Bogotá, Colombia
[b] UNESP – Universidade Estadual Paulista, Departamento de Física, Caixa Postal 473, Bauru, SP, Brazil
[c] UNESP – Universidade Estadual Paulista, IPMet – Instituto de Pesquisas Meteorológicas, CEP 17048-699 Bauru, SP, Brazil
[d] Departamento de Física, Universidade Federal de Pernambuco, CEP 50670-901, Recife, PE, Brazil

ARTICLE INFO

Article history:
Received 16 October 2014
Received in revised form 12 December 2014
Accepted 16 December 2014
Available online 23 December 2014
Communicated by L. Ghivelder

Keywords:
Vortex
Ginzburg–Landau
Mesoscopic
Pillars

ABSTRACT

We theoretically investigate the local magnetic field, order parameter and supercurrent profiles of a parallelepiped mesoscopic superconductor submersed in an applied magnetic field; this same geometry with a pillar on its top surface is also considered. Our investigation was carried out by solving the three-dimensional time-dependent Ginzburg–Landau (TDGL) equations. We obtain the magnetization curve as a function of the external applied magnetic field for several sample sizes. We have determined an analytical dependence of the thermodynamic fields and the magnetization as functions of the lateral dimension of the superconductor. Finally, a systematic comparative study of the two- and three-dimensional approaches of the Ginzburg–Landau model is carried out.

1. Introduction

It is well known that quantum confinement effects in superconductors become important when the size of the sample is comparable to the coherence length $\xi(T)$ or to the London penetration depth $\lambda(T)$; T is the temperature. In particular, as a consequence of the demagnetization effects, when the size of the sample along the direction of the applied magnetic field is smaller than the lateral dimensions of its cross section, the local magnetic field near the edges of the sample is enhanced and interacts with the shielding currents. There are many experimental (see for instance [1–5]) and theoretical (see for instance [6–10]) studies in three-dimensional (3D) systems. For example, in [11], a superconducting wire with a constriction in the middle was investigated. It was found that, when a giant-vortex is nucleated in the widest part of the wire, it can break up into a smaller giant and/or individual vortices near the constriction. In all these theoretical studies, the Ginzburg–Landau model has been proven to give a good account of the superconducting properties in samples of several geometries, i.e., disks with finite height and spheres [12,13], shells [14], cone [15], prism with arbitrary base and a solid of revolution with arbitrary profile [16], thin circular sectors and thin disks [17,18], among others. The local magnetic field profile of a mesoscopic superconductor in the so-called SQUID (superconducting quantum interference device) geometry was studied using the 3D approach [19]. These systems are very important in the fabrication and development of microwave circuits and atom chips [20,21] and in the SQUID production [22]. The limit below which a parallelepiped superconductor of cross section area $S = 9\xi^2$ should be described by the 3D Ginzburg–Landau model corresponds to the thickness $d \leq 8\xi$. For any value above this limit, the magnetization curve approximates the characteristic curve for $d \to \infty$ case, for which the local magnetic field and the order parameter are invariant along the z-direction [23,24]; we refer to this limit as two-dimensional (2D). In this work we studied the superconducting properties of a parallelepiped sample of volume $V = l^2 d$, where l and d are the lateral size and thickness of the sample, respectively, by using the 3D TDGL equations. We calculate the magnetization, free energy, vorticity and Cooper pair density. We also will make a systematic comparison between the outcome both from the 2D and 3D simulations. Normally, the 2D approach of the Ginzburg–Landau equations is useful in obtaining some insight of the main physical properties of a superconductor. However, we will show that it is not capable of fully extracting very important physical

* Corresponding author.
E-mail address: josejbarba@gmail.com (J. Barba-Ortega).

http://dx.doi.org/10.1016/j.physleta.2014.12.030
0375-9601/

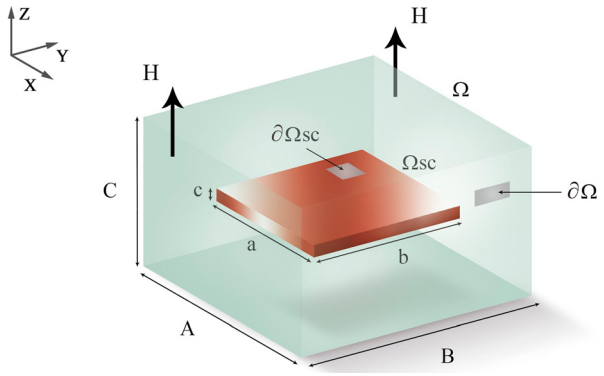

Fig. 1. (Color online.) Schematic view of the geometry of the system under investigation.

issues of the superconducting state such as the vortex configurations and the irreversibility of the magnetization curve.

The understanding of the vortex state and how vortices interact with each other is a basic issue previously applied to the study of more complex dynamical effects such as superconductors in the presence of transport currents. Vortex–vortex interaction, both in bulk and very thin superconductors, is well known since a long time ago [25,26]. For bulk superconductors this interaction is short-range, rather than long-range for films. However, for very confined geometries (l of order of a few ξ's and d of order ξ) this is still an open issue. In this paper, we will not propose any new vortex–vortex interaction for mesoscopic superconductors, but we will show that the choice of approach, either 2D or 3D, may be a crucial step towards this audacious aim.

2. The theoretical formalism

2.1. The system geometry

The geometry of the problem that we investigate is illustrated in Fig. 1. The domain Ω_{sc} covers the mesoscopic superconducting parallelepiped of thickness c and lateral sizes a and b. The interface between this region and the vacuum is denoted by $\partial\Omega_{sc}$. Because of the demagnetization effects, we need to consider a larger domain Ω of dimensions $A \times B \times C$, such that $\Omega_{sc} \subset \Omega$. The vacuum–vacuum interface is indicated by $\partial\Omega$. Fig. 1 is sketched for any parallelepiped, although here we will consider the special case $A = B = L$, $C = D$, $a = b = l$, and $c = d$.

Now, suppose that the superconductor is immersed in a uniformly applied magnetic field $\mathbf{H}$. The presence of the superconductor will modify the profile of the local magnetic field near the edges. Here, we consider the dimensions of Ω sufficiently large such that the local magnetic field equals the external applied magnetic field $\mathbf{H}$ at the interface $\partial\Omega$ (see Fig. 1).

Another variant of this system which will be studied here is the introduction of a pillar of dimensions $W \times W \times a$ on the top of the parallelepiped as shown in Fig. 2. For simplicity, in this figure, we show only the superconducting domain Ω_{sc}. It is implicit that the parallelepiped plus the pillar are inside the larger domain Ω.

2.2. The 3D Ginzburg–Landau model

Our starting point is the TDGL equations which describe the superconducting state. They are two coupled partial differential equations, one for the order parameter ψ and another one for the vector potential $\mathbf{A}$ which is related to the local magnetic field through the expression $\mathbf{h} = \nabla \times \mathbf{A}$. We have:

$$\frac{\partial\psi}{\partial t} = -(-i\nabla - \mathbf{A})^2\psi + \psi\left(1 - |\psi|^2\right), \quad \text{in } \Omega_{sc}, \tag{1}$$

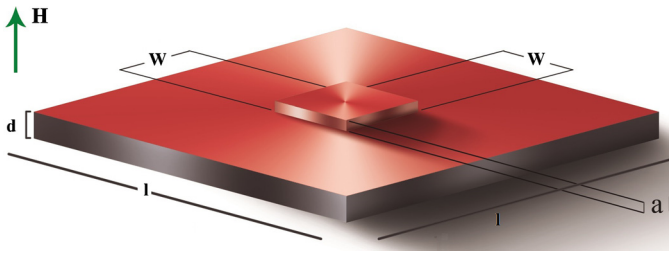

Fig. 2. (Color online.) Schematic view of a superconducting parallelepiped with a pillar on the top.

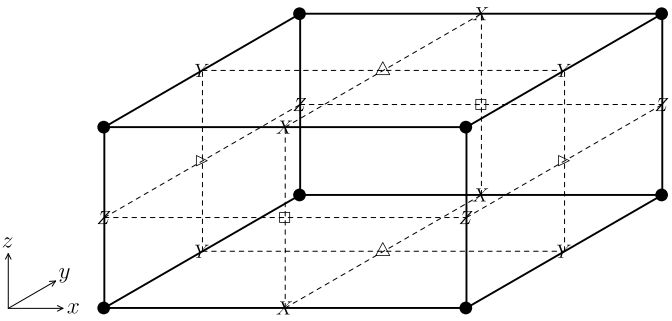

Fig. 3. Evaluation point for ψ (●), A_x and J_{sx} (X), A_y and J_{sy} (Y), A_z and J_{sz} (Z), h_x (▷), h_y (△), h_x (□).

$$\frac{\partial\mathbf{A}}{\partial t} = \begin{cases} \mathbf{J}_s - \kappa^2\nabla\times\nabla\times\mathbf{A}, & \text{in } \Omega_{sc}, \\ -\kappa^2\nabla\times\nabla\times\mathbf{A}, & \text{in } \Omega\backslash\Omega_{sc}, \end{cases} \tag{2}$$

$$\mathbf{J}_s = \mathrm{Re}\left[\bar{\psi}(-i\nabla - \mathbf{A})\psi\right], \tag{3}$$

where $\mathbf{J}_s$ is the supercurrent density. As we have stated previously, the domain Ω must be sufficiently large such that the local magnetic field $\mathbf{h} = \nabla \times \mathbf{A}$ equals the applied field $\mathbf{H}$ far away from Ω_{sc}. We impose that the current density does not flow out of the superconductor into the vacuum. This means that the perpendicular component of $\mathbf{J}_s$ vanishes at the $\partial\Omega_{sc}$ surface. Let us denote by $\mathbf{n}$ the unit vector outward normal to the superconductor-vacuum interface. Then, Eqs. (1) and (2) satisfy the following boundary conditions:

$$\mathbf{n}\cdot(i\nabla + \mathbf{A})\psi = 0, \quad \text{at } \partial\Omega_{sc}, \tag{4}$$

$$\nabla\times\mathbf{A} = \mathbf{H}, \quad \text{at } \partial\Omega. \tag{5}$$

In Eqs. (1)–(3) dimensionless units were introduced as follows: the order parameter in units of $\psi_\infty(T) = \sqrt{-\alpha(T)/\beta}$, where $\alpha(T)$ and β are two phenomenological constants; T in units of the critical temperature T_c; lengths in units of the coherence length ξ; time in units of $t_0 = \pi\hbar/8K_BT_c$; the vector potential $\mathbf{A}$ in units of ξH_{c2}, where H_{c2} is the bulk second critical field; Gibbs free energy G in units of $G_0 = H_{c2}^2V/8\pi$ [27]; $\kappa = \xi/\lambda$ is the Ginzburg–Landau parameter.

In order to solve Eqs. (1)–(3) numerically, we used the link-variable method as sketched in references [28,29].[1] Here, we provide a brief description of the numerical setup. The domain Ω is subdivided in $N_x \times N_y \times N_z$ unit cells of dimensions $\Delta x \times \Delta y \times \Delta z$, where $N_x = L/\Delta x$, $N_y = L/\Delta y$, and $N_z = D/\Delta z$. In Fig. 3 we show one grid cell of the domain Ω_{sc} and the evaluation points for all physical quantities. A grid cell outside the superconducting domain is the same, except by the fact that it does not include the evaluation points for the order parameter and the supercurrent

[1] Although we used the TDGL equations, we are concerned only with the stationary state; they are used only as a relaxation method towards the equilibrium state.

density. The discretization procedure of Eqs. (1)–(3), supplied by the boundary conditions (4)–(5), leads us to a set of recurrence relations for the order parameter and the components of the vector potential at different time steps (explicit Euler method). We run these equations starting from zero applied field and the Meissner state for which $\psi = 1$ everywhere in Ω_{sc}. Then, we increase adiabatically the external applied field H in small steps ΔH, until superconductivity is completely destroyed. At each step we let the system attain its equilibrium configuration and use such state as the initial condition for the next applied field.

2.3. The 2D Ginzburg–Landau model

Suppose now that the system has invariance along the z-direction and the external magnetic field is applied along the same direction; this is the case of a long cylinder, either of circular or rectangular cross section. Within this scenario, the problem becomes 2D for which the physical quantities vary only with the x and y coordinates and demagnetization effects are not present, that is, the local magnetic field outside the sample is the external applied magnetic field $\mathbf{H}$ everywhere. In this case, the TDGL equations (1)–(3) are essentially the same, except by the fact that now they are solved only in Ω_{sc} and, $\psi = \psi(x, y)$, $\mathbf{A} = A_x(x, y)\mathbf{i} + A_y(x, y)\mathbf{j}$ and $\mathbf{h} = h_z(x, y)\mathbf{k}$. The boundary condition (4) remains unchanged. However, Eq. (5) becomes $\nabla \times \mathbf{A} = \mathbf{H}$, at $\partial\Omega_{sc}$.

The numerical setup to solve the 2D TDGL equations is similar to the 3D counterpart, although it is much simpler. The difference now is that we run the recurrence relations for the order parameter and the vector potential only in one rectangle mesh grid with $n_x \times n_y$ unit cells, where $n_x = l/\Delta x$, $n_y = l/\Delta y$.

The 2D TDGL equations are also employed to study films of very small thickness with variable surface, but with an adaption which we discuss below. Usually this problem is treated from the theoretical point of view by considering the film thickness less than ξ. The order parameter is supposed not to vary along the z-direction inside the film. Then, the 3D TDGL equations are averaged along the z-direction and the problem turns into a 2D one where all physical quantities depend only on the (x, y) coordinates [8,30]. One has:

$$\frac{\partial\psi}{\partial t} = -(-i\nabla - \mathbf{A})^2\psi + \psi\left(1 - |\psi|^2\right) + i(-i\nabla - \mathbf{A}) \cdot \frac{\nabla g}{g}, \quad \text{in } \Omega_{sc}, \tag{6}$$

where $0 < g(x, y) \leq \xi$ is a function which is given by d everywhere, except in the pillar region where is $d + a \leq \xi$. The 2D equations for the vector potential and the supercurrent density remain unchanged.

2.4. Numerical comparison between the two models

From the discussion above we see that to solve the 2D TDGL equations numerically we just need a rectangular mesh grid of $(n_x + 1) \times (n_y + 1)$ points, whereas for the 3D equations we need $(N_z + 1)$ larger planes, each having $(N_x + 1) \times (N_y + 1)$ points. This hugely increases the computational time to obtain the state for each value of H.

The total simulation time to obtain the hysteresis loop of the magnetization and energy as functions of the external applied magnetic field depends on the time step which guarantees the stability of the numerical TDGL equations (see for instance [28]). If the $\Delta x = \Delta y = \Delta z$, then the time step is given by[2]:

$$\Delta t = \min\left\{\frac{\Delta x^2}{4}, \frac{\Delta x^2}{4\kappa^2}\right\}. \tag{7}$$

If $\kappa \gg 1$ ($\kappa \ll 1$) we penalize the convergence of the second (first) TDGL equation. Since the computational time to achieve the stationary state for the 3D model is much larger than for the 2D one, we have chosen the parameter $\kappa = 1$. The ideal scenario would carry out a study for several values of κ. However, having in mind this serious technical limitation we had to keep κ fixed at a conveniently value and vary only the dimensions of the superconductor.

The 2D approach is quite frequently used to describe physical systems, even for films of very small thickness. It has been proven that this approximation is reasonable for very high κ limit [8]. Although we can gain a good picture of the physical scenario, in what follows, we will show that, for finite κ, these simplifications may compromise the description of the electronic and structural properties of the mesoscopic superconductors (see Section 3).

3. Results and discussion

We have studied a mesoscopic superconducting parallelepiped of height $d = 1\xi$ and several values of the lateral dimension L; in the numerical simulations we employed the Ginzburg–Landau parameter as $\kappa = 1.0$. In order to solve the true 3D Ginzburg–Landau equations, the size of the simulation box Ω was taken with the following dimensions $19\xi \times 19\xi \times 11\xi$ while the superconductor inside, domain Ω_{sc}, has the size $L \times L \times 1\xi$, with the lateral dimensions assuming the values $L = 3\xi, 6\xi, 9\xi, 12\xi$. The grid space used was $\Delta x = \Delta y = \Delta z = 0.1$.

In Section 3.1 a parallelepiped is studied by assuming its top surface as flat and in Section 3.2 we consider a pillar on its top.

3.1. Superconducting parallelepiped

In Fig. 4 we illustrate the magnetization $4\pi M$ (upper panels), the Gibbs free energy G (middle panels), and the vorticity N (lower panels) as functions of the external field H, by increasing and then decreasing it. In the inset of the middle and lower panels we show some snapshots of the order parameter and the supercurrent density at the indicated values in the curves (green symbols). The phase of the order parameter allows to determine the number of vortices in a given closed path. If the vorticity in this region is N, then the phase changes by $2\pi N$. As we can see from Fig. 4, for $l = 6\xi$, a giant-vortex with vorticity $N = 2$ at the center of the film is formed when the external applied magnetic field is increasing (a) and a multi-vortex state $N = 4$ when the external applied magnetic field is decreasing (b). On the other hand, for $l = 12\xi$ a multi-vortex state is formed with $N = 4$ when the external applied magnetic field is increasing (c) and a multi-vortex state $N = 8$ when the external applied magnetic field is decreasing (d). For l sufficiently large we have giant-vortex coexisting with multi-vortex state only for large vorticities. We also show the supercurrent density vector field in the lower panels of Fig. 4. All the transitions are presented in the N versus H curves. As we will see later on, the dynamics of nucleation of vortices in the 3D and 2D Ginzburg–Landau models are rather different.

We have found somewhere else the estimated minimum size of the superconductor for which just one vortex is present [23]. We found that $L = 3\xi$. This is not different for the 2D scenario [31]. Since for both films of finite thickness (3D) and very long cylinders (2D) the vortex–vortex interaction is repulsive, this result is rather expected because what really matters in this case is the area of the square cross section of the superconductor to accommodate one quantum of flux rather than the length of the system along the z-direction.

[2] Larger time steps can be used by using implicit methods. But usually they are very difficult to implement, specially for the 3D TDGL model.

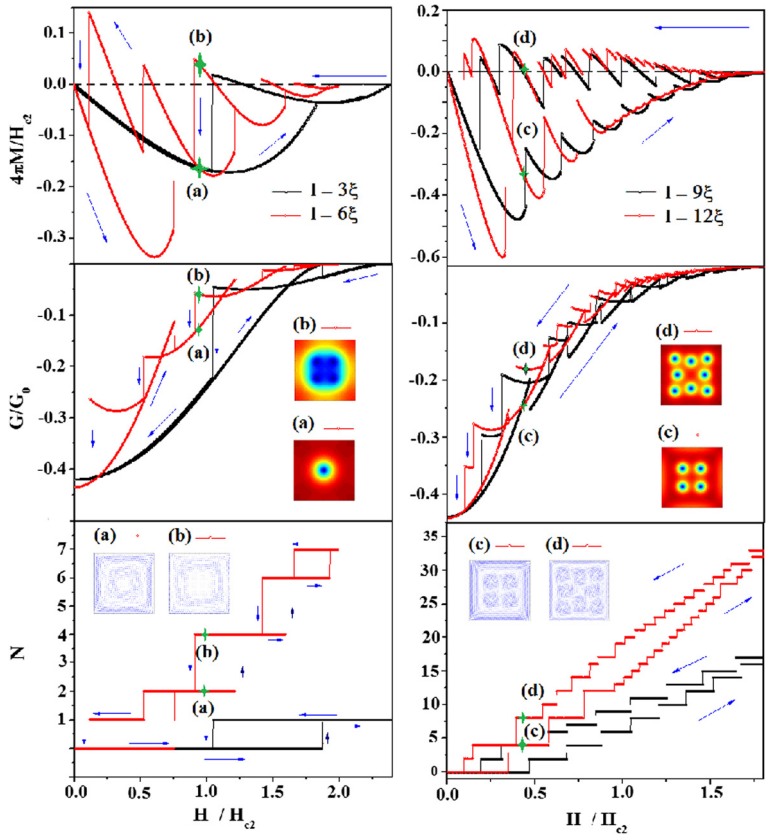

Fig. 4. (Color online.) The magnetization $4\pi M$ (upper panels), the Gibbs free energy G (middle panels), and the vorticity N (lower panels) as functions of the external applied magnetic field H_1 for both upward and downward branches, for $l/\xi = 3$ and 6 (left column), and $l/\xi = 9$ and 12 (right column). Insets: the order parameter and the supercurrent density for $H = 0.96H_{c2}$ and $l/\xi = 6$ (left column), and for $H = 0.46H_{c2}$ and $l/\xi = 12$ (right column). The green symbols on the curves indicate the external applied field under consideration.

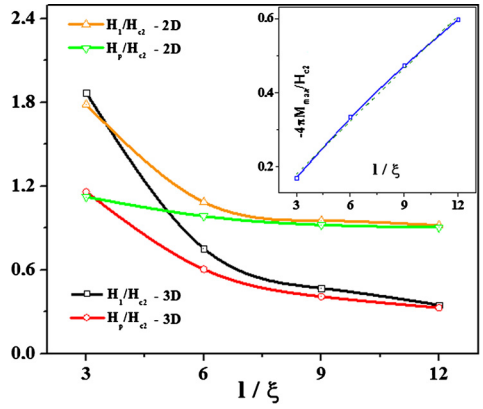

Fig. 5. (Color online.) First vortex penetration field, H_1, and the external applied field for which the maximum of the magnetization $-4\pi M$ occurs, H_p, as a functions of l for both the 2D and 3D geometries. Inset: the maximum of the magnetization $-4\pi M_{\max}$ at $H = H_p$ as a function of l; the dashed line corresponds to the fitting of the data shown by the blue line which corresponds only for the 3D simulations.

We have gone further by analyzing the diamagnetic properties of the superconductor both from the 3D and 2D perspective (see Fig. 5). It is well known that films usually have the first nucleation field lower than for very thick samples. However, to our best knowledge this has not been quantified yet, at least for mesoscopic superconductors. In Fig. 5 we present the values of the first penetration field, H_1, and the field corresponding to the maximum of $-4\pi M$, H_p, as functions of l/ξ, both for 3D and 2D samples. As we can observe, for $l \geq 6\xi$, both fields have significantly larger values for 2D samples. This is a very strong indication (among others which will be pointed out later on) that the 2D approach to investigate the superconducting films may not be entirely reliable. Still concerning Fig. 4, we plotted the linear fitting $-4\pi M_{\max} \approx 0.047L + 0.039$ and the exponential ones $H_1 \approx 0.028 + 5.472\exp(-l/2.369)$ and $H_p \approx 0.287 + 2.386\exp(-l/2.976)$, with l in units of ξ. This has been done only for one value of κ. So, we cannot assure that this fitting is valid for higher values of κ, once the larger it is the lesser is the first penetration field.

Let us now turn our discussion to the vortex configurations. In Fig. 6 we depict the modulus of the order parameter, as a density plot, and the local magnetic field for the same value of the external applied magnetic field on both upward and downward branches. All these plots are for $|\psi|$ and h_z taken at the $z = 0$ plane. From Fig. 6 we can see that for $l = 6\xi$ we have an $N = 2$ giant-vortex state in both branches of the external applied magnetic field. This has also been found by using the 2D approach by many authors (see for instance [32,33]). The cases $l = 9\xi, 12\xi$ present multi-vortex states with $N = 4, 12$, respectively, in the upward branch and $N = 9, 16$, respectively, in the downward branch of the external applied magnetic field. Notice that in both situations, the vortices tend to accommodate into a configuration which follows the geometry of the sample, that is, a square lattice. There are two ingredients influencing on the formation of the lattice: the vortex–vortex interaction which is repulsive, and the vortex–surface interaction; this last one is related to the Lorentz force which pushes the vortex to the interior of the sample, once it has been nucleated. From this balance it will result the vortex state. Later on, we will see that the 2D approach produces distinct pictures.

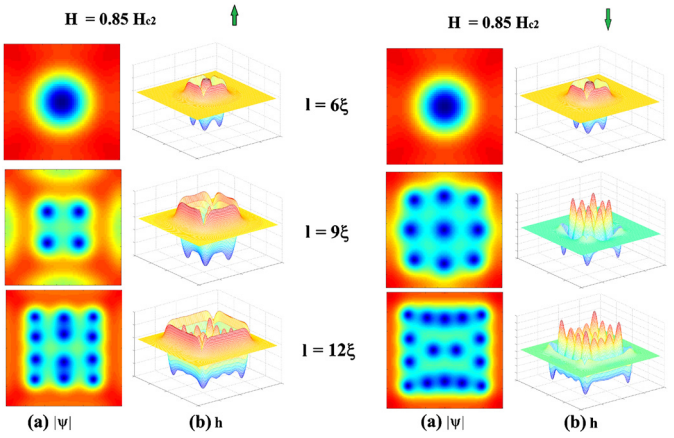

Fig. 6. (Color online.) Spatial pattern of: (a) modulus of the order parameter and (b) the z-component of the local magnetic **h**, in the upward branch (panels of the two left columns) and the downward branch (panels of the two right columns) for the indicated values of l/ξ and $H = 0.85H_{c2}$.

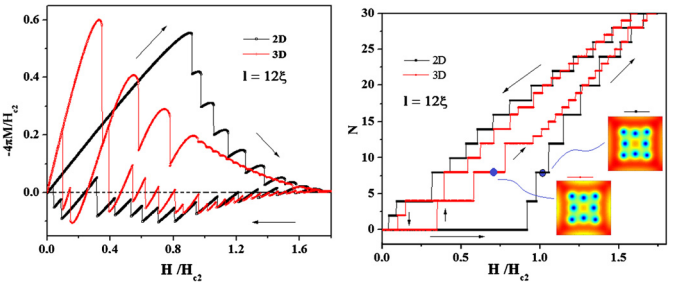

Fig. 7. (Color online.) The magnetization $-4\pi M$ (left panel) and the vorticity N (right panel) as functions of the external applied field for both the 2D and 3D outcome.

In Fig. 6, notice the strong demagnetization effects of the local field near the border of the sample in both branches of H. This effect, present only in 3D models, has a very important influence on the magnetization signal of Fig. 4. Since the local magnetic field is strengthened on the edge of the sample, the first nucleation field occurs at smaller values than predicted by the 2D model. In Fig. 7 we compare the magnetization and vorticity curves coming from both 2D and 3D simulations; the parameters used are specified in the figure. We see that the value of $H_{1,2D}$ is much larger than $H_{1,3D}$. On the other hand, in the downward branch, we can observe that the paramagnetic signal is slightly stronger in the 2D magnetization curve than in the 3D equivalent one. These different behaviors can be explained by the demagnetization effect which precipitates the first vortex penetration and facilitates the escaping of flux quantum by decreasing H. As we have mentioned early, this produces a rather different vortex dynamic.

One difficulty in making a comparison between the 2D and 3D models on equal footing comes from the fact that most of the configurations with equal vorticity N belongs to distinct values of the external applied magnetic field. In the right panel of Fig. 7 we see that the $N = 8$ vortex states are very similar in both models, although the respective values of H are quite different. This is so, because in the 2D model, the absence of demagnetization effect requires a larger external applied field to enhance the shielding currents and consequently produces the same picture observed in the 3D model at a larger value of H. On the other hand, for larger vorticity, the higher values of H are not sufficient to compensate the lack of demagnetization effects in producing the same vortex state. This can be seen in Fig. 8 where we depict the order parameter intensity for some vorticities. For instance, in the right panels

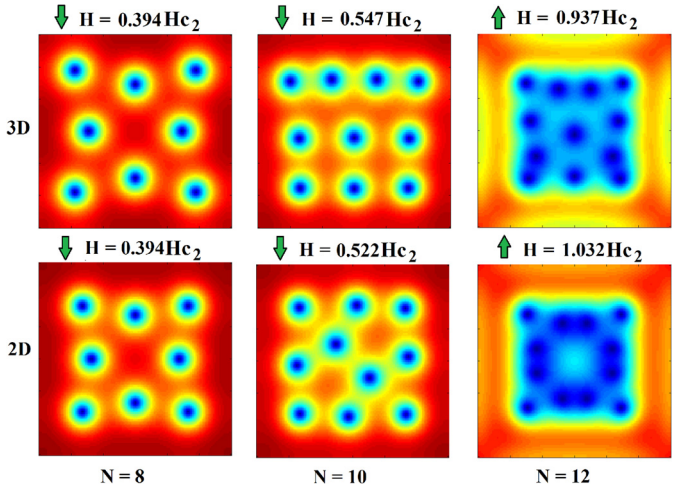

Fig. 8. (Color online.) The modulus of the order parameter: a comparative study between the 2D and 3D models.

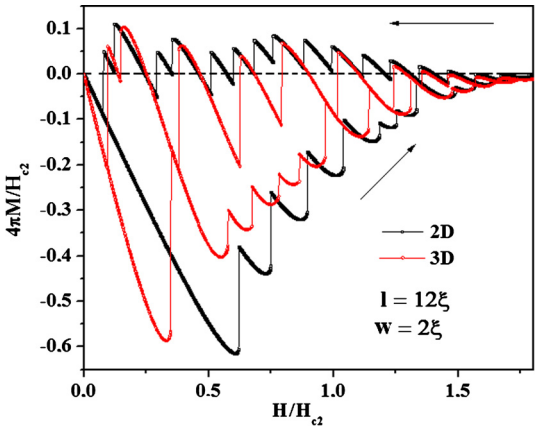

Fig. 9. (Color online.) The magnetization $-4\pi M$ as a function of the external applied field for a superconductor with a pillar on its top, both for the 2D and 3D models.

of Fig. 8, for $N = 12$ we illustrate the dissimilarities of the 2D and 3D vortex configurations.

Fortunately, in the downward branch, we have found some situations in which the values of H are very close for a common vorticity N. As it can be seen in the left panels of Fig. 8, for $N = 8$ and the same value $H = 0.394H_{c2}$ the vortex configurations are exactly the same, although in the 3D picture the vortices are more distant from one each other, because the shielding currents are weaker with respect to the 2D counterpart. For $N = 10$, even for slightly different H values, we see that the vortex states are very distinct.

3.2. Superconducting parallelepiped with a pillar

We have taken the following parameters for the pillar: $l = 12\xi$, $d = 0.5\xi$ and the dimensions of the pillar as $W = 2\xi$ and $a = 0.5\xi$ in order to satisfy the constraint $g(x, y) \leq \xi$ for the 2D Ginzburg–Landau model. The size of the simulation box Ω is the same as before.

First of all, with respect to the values of $H_{1,2D}$ and $H_{1,3D}$, we have found that the presence of the pillar perturbation diminishes the difference of the first penetration field, $\Delta H_1 = H_{1,2D} - H_{1,3D}$, from approximately $0.6H_{c2}$ to $0.3H_{c2}$ (see Figs. 7 and 9). This makes easier the comparison between the two models with respect to the case of no pillar. In Fig. 10 we show some snapshots of the modulus of the order parameter on the $z = d/2$ plane, which corresponds to the top of the film.

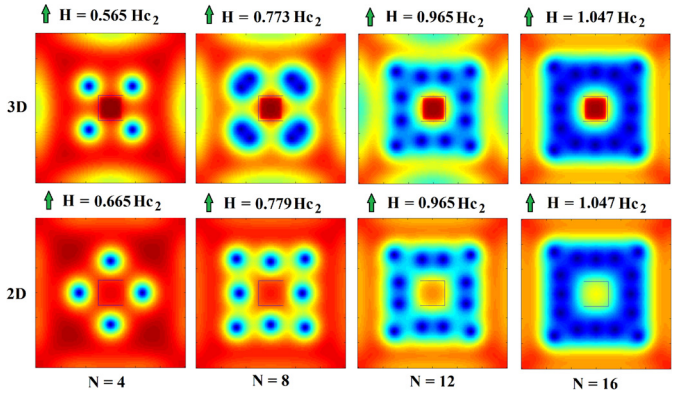

Fig. 10. (Color online.) The order parameter intensity: a comparative study between the 2D and 3D models for the case of parallelepiped with a pillar on its top. The pillar basis is indicated by the square at the center.

Beyond the differences of the vortex configurations, we have found additional distinct characteristic of the superconducting state originating from the two approaches of the Ginzburg–Landau equations. From Fig. 10 we can see that in the $N = 4, 8$ states for the 3D model, the vortices are more attracted by the corners of the pillar, whereas, for the 2D model they are repelled. This difference is also present for larger N, although less evident. Of course we should be cautions in generalizing this finding, since it may depend on the size of the pillar. Another interesting characteristic is that inside the pillar, the superconductivity is less destroyed in the 3D model than in its 2D counterpart. Further studies with many pillars are underway and will be reported elsewhere.

4. Conclusions

We studied the thermodynamics properties of a three-dimensional small superconducting parallelepiped in the presence of an external applied magnetic field by solving the non-linear Ginzburg–Landau equations. Our results show that the numerical simulations used to investigate the structural and magnetic properties of the vortex matter critically depend on the choice among the 2D and 3D approaches of the Ginzburg–Landau equations if the thickness of the sample is finite.

Acknowledgements

E.S. thanks the Brazil agency FAPESP for financial support (grant 2012/04388-00), and J.A.A. thanks the Brazilian science agencies CNPq (grants 307552/2012-8 and 141911/2012-3), and FACEPE (AMD-0088-1.05/13 and grant APQ-0589/1.05-08) for supporting this research.

References

[1] H. Kupfer, G. Linker, G. Ravikumar, T. Wolf, A. Will, A. Zhukov, R. Meier-Hirmer, B. Obst, H. Wuh, Phys. Rev. B 67 (2003) 064507.
[2] E.T. Filby, A.A. Zhukov, P.A.J. de Groot, M.A. Ghanem, P.N. Bartlett, V.V. Metlushko, Appl. Phys. Lett. 89 (2006) 092503.
[3] Z.L. Xiao, C. Han, W.K. Kwok, H.H. Wang, U. Welp, J. Wang, G. Crabtree, J. Am. Chem. Soc. (Communications) 126 (2004) 2316.
[4] R.I. Rey, A.R. Alvarez, C. Carballeira, J. Mosqueira, F. Vidal, S. Salem, A.D. Alvarenga, R. Zhang, H. Luo, Supercond. Sci. Technol. 27 (2014) 075001.
[5] H. Suderow, I. Guillamon, J.G. Rodrigo, S. Vieira, Supercond. Sci. Technol. 27 (2014) 063001.
[6] D. Glotov, Z. Angew. Math. Phys. 62 (2011) 891.
[7] Q. Du, M.D. Gunzburger, Physica D 69 (1993) 215.
[8] S.J. Chapman, Q. Du, M.D. Gunzburger, Z. Angew. Math. Phys. 47 (1993) 410.
[9] G.R. Berdiyorov, M.M. Doria, A.R. de C. Romaguera, M.V. Milosevic, E.H. Brandt, F.M. Peeters, Phys. Rev. B 87 (2013) 184508.
[10] L.F. Zhang, L. Covaci, M.V. Milosevic, G.R. Berdiyorov, F.M. Peeters, Phys. Rev. Lett. 109 (2012) 107001.
[11] A.K. Elmurodov, D.Y. Vodolazov, F.M. Peeters, Europhys. Lett. 74 (2006) 151.
[12] B. Xu, M.V. Milosevic, F.M. Peeters, Phys. Rev. B 77 (2008) 144509.
[13] M.M. Doria, R.M. Romaguera, F.M. Peeters, Phys. Rev. B 75 (2007) 064505.
[14] Q. Du, J. Math. Phys. 46 (2005) 095109.
[15] Y. Chen, M.M. Doria, F.M. Peeters, Phys. Rev. B 77 (2008) 054511.
[16] P.J. Pereira, V.V. Moshchalkov, L.F. Chibotaru, J. Phys. Conf. Ser. 490 (2014) 01222.
[17] J. Barba-Ortega, J.D. Gonzalez, E. Sardella, J. Low Temp. Phys. 174 (2014) 96.
[18] J. Barba-Ortega, E. Sardella, J.A. Aguiar, Supercond. Sci. Technol. 24 (2011) 015001.
[19] F. Rogeri, R. Zadorosny, P.N. Lisboa-Filho, E. Sardella, W.A. Ortiz, Supercond. Sci. Technol. 26 (2013) 075005.
[20] N. Klein, Appl. Phys. Lett. 5 (1964) 65.
[21] V. Sokolovsky, L. Prigozhin, V. Dikovsky, Supercond. Sci. Technol. 23 (2010) 065003.
[22] H.J. Brake, Physica C 439 (2006) 1.
[23] J. Barba-Ortega, J.D. Gonzalez, E. Sardella, J. Low Temp. Phys. 177 (2014) 193.
[24] L.F. Zhang, L. Covaci, M.V. Milosevic, G.R. Berdiyorov, F.M. Peeters, Phys. Rev. B 88 (2013) 144501.
[25] A.A. Abrikosov, Sov. Phys. JETP 5 (1957) 1174.
[26] J. Pearl, Appl. Phys. Lett. 5 (1964) 65.
[27] E. Zeldov, A.I. Larkin, V.B. Geshkenbein, M. Konczykowski, D. Majer, B. Khaykovich, V.M. Vinokur, H. Shtrikman, Phys. Rev. Lett. 73 (1994) 1428.
[28] W.D. Gropp, H.G. Kaper, G.K. Leaf, D.M. Levine, M. Palumbo, V.M. Vinokur, J. Comput. Phys. 123 (1994) 254.
[29] G. Buscaglia, C. Bolech, C. Lopez, in: J. Berger, J. Rubinstein (Eds.), Connectivity and Superconductivity, Springer, Heidelberg, 2000.
[30] G.R. Berdiyorov, V.R. Misko, M.V. Milosevic, W. Escoffier, I.V. Grigorieva, F.M. Peeters, Phys. Rev. B 77 (2008) 024526.
[31] P.N. Lisboa-Filho, A.L. Malvezzi, E. Sardella, Phys. Rev. B 403 (2008) 1494.
[32] B.J. Baelus, F.M. Peeters, Phys. Rev. B 65 (2002) 104515.
[33] E. Sardella, A.L. Malvezzi, P.N. Lisboa-Filho, W.A. Ortiz, Phys. Rev. B 74 (2006) 014512.